



MAX-PLANCK-INSTITUT FÜR PHYSIK UND ASTROPHYSIK

WERNER-HEISENBERG-INSTITUT FÜR PHYSIK

MPI-PAE/Exp.E1. 168
December 1986

A MEASUREMENT OF DIRECT PHOTON PRODUCTION
AT LARGE TRANSVERSE MOMENTUM
IN π^-p , π^+p AND pp COLLISIONS AT 300 GeV/c

C. DE MARZO, M. DE PALMA, C. FAVUZZI, G. MAGGI, E. NAPPI,
F. POSA, A. RANIERI, G. SELVAGGI AND P. SPINELLI
DIPARTIMENTO DI FISICA DELL'UNIVERSITA DI BARI
AND ISTITUTO NAZIONALE DI FISICA NUCLEARE, BARI, ITALY

A. BAMBERGER, M. FUCHS, W. HECK, C. LOOS, R. MARX, K. RUNGE,
E. SKODZEK, C. WEBER, M. WÜLKER AND F. ZETSCHKE
UNIVERSITY OF FREIBURG, FREIBURG, GERMANY

V. ARTEMIEV, YU. GALAKTIONOV, A. GORDEEV, YU. GORODKOV,
YU. KAMYSHKOV, V. PLYASKIN, V. POJIDAEV,
V. SHEVCHENKO, E. SHUMILOV AND V. TCHUDAKOV
ITEP, MOSCOW, U.S.S.R.

J. BUNN*, J. FENT, P. FREUND, J. GEBAUER, M. GLAS, P. POLAKOS**,
K. PRETZL, T. SCHOUTEN***, P. SEYBOTH,
J. SEYERLEIN AND G. VESZTERGOMBI****
MAX-PLANCK-INSTITUT FÜR PHYSIK UND ASTROPHYSIK,
MÜNCHEN, GERMANY

NA24-COLLABORATION

submitted to Phys. Rev. D

*PRESENT ADDRESS: CERN, GENEVA (SWITZERLAND)

**PRESENT ADDRESS: BELL LABS HOLMDEL, NEW JERSEY (U.S.A.)

***PRESENT ADDRESS: UNIVERSITY OF NIJMEGEN (NETHERLANDS)

****ON LEAVE OF ABSENCE FROM CENTRAL RESEARCH INSTITUTE FOR PHYSICS, BUDAPEST
(HUNGARY)

Alle Rechte vorbehalten

Max-Planck-Institut für Physik und Astrophysik, München.

**A MEASUREMENT OF DIRECT PHOTON PRODUCTION
AT LARGE TRANSVERSE MOMENTUM
IN π^-p , π^+p AND pp COLLISIONS AT 300 GeV/c**

C. DE MARZO, M. DE PALMA, C. FAVUZZI, G. MAGGI, E. NAPPI,
F. POSA, A. RANIERI, G. SELVAGGI AND P. SPINELLI
DIPARTIMENTO DI FISICA DELL'UNIVERSITA DI BARI
AND ISTITUTO NAZIONALE DI FISICA NUCLEARE, BARI, ITALY

A. BAMBERGER, M. FUCHS, W. HECK, C. LOOS, R. MARX, K. RUNGE,
E. SKODZEK, C. WEBER, M. WÜLKER AND F. ZETSCHKE
UNIVERSITY OF FREIBURG, FREIBURG, GERMANY

V. ARTEMIEV, YU. GALAKTIONOV, A. GORDEEV, YU. GORODKOV,
YU. KAMYSHKOV, V. PLYASKIN, V. POJIDAEV,
V. SHEVCHENKO, E. SHUMILOV AND V. TCHUDAKOV
ITEP, MOSCOW, U.S.S.R.

J. BUNN*, J. FENT, P. FREUND, J. GEBAUER, M. GLAS, P. POLAKOS**
K. PRETZL, T. SCHOUTEN***, P. SEYBOTH,
J. SEYERLEIN AND G. VESZTERGOMBI****
MAX-PLANCK-INSTITUT FÜR PHYSIK UND ASTROPHYSIK,
MÜNCHEN, GERMANY

NA24-COLLABORATION

Abstract

Cross sections for inclusive direct photon production in π^-p , π^+p and pp collisions at 300 GeV/c are measured at transverse momenta, p_T , up to 7 GeV/c ($x_T=0.6$). For $\pi^-p \rightarrow \gamma X$ also the rapidity distribution is presented. The cross section ratio $\sigma(\pi^-p \rightarrow \gamma X)/\sigma(\pi^+p \rightarrow \gamma X)$ is found to be one at $p_T = 4$ GeV/c and rises with increasing p_T . This observation signals the occurrence of valence quark antiquark annihilation. The results are in good agreement with QCD predictions.

*PRESENT ADDRESS: CERN, GENEVA (SWITZERLAND)

**PRESENT ADDRESS: BELL LABS HOLMDEL, NEW JERSEY (U.S.A)

***PRESENT ADDRESS: UNIVERSITY OF NIJMEGEN (NETHERLANDS)

****ON LEAVE OF ABSENCE FROM CENTRAL RESEARCH INSTITUTE FOR PHYSICS, BUDAPEST (HUNGARY)

1. Introduction

The measurement of direct photon production at high transverse momentum, p_T , in hadron-hadron collisions reveals rather clean information about constituent scattering dynamics since the photon directly probes the small distance behaviour of the interaction [1].

Direct photon production was first measured in pA and in pp collisions [2]. Here the dominant contribution to the direct photon yield stems from the QCD-Compton scattering process $qg \rightarrow \gamma q$.

This experiment has studied the direct photon production in $\pi^- p$, $\pi^+ p$ and pp collisions at 300 GeV/c as a function of p_T and rapidity. With incident π^\mp beams the valence quark-antiquark annihilation process $q\bar{q} \rightarrow \gamma g$ also becomes accessible due to the antiquark content in the projectile pion. QCD predicts the annihilation process to dominate over the QCD-Compton process at large p_T . One further expects the direct photon yield in $\pi^- p$ collisions to be larger than in $\pi^+ p$ collisions due to the charges of the antiquarks and the number of annihilation partners involved. The observation of a rising cross section ratio $\sigma(\pi^- p \rightarrow \gamma + X)/\sigma(\pi^+ p \rightarrow \gamma + X)$ with increasing p_T will therefore signal the occurrence of valence quark-antiquark annihilations.

Precise measurements of the direct photon cross sections and cross section ratios provide a good testing ground for QCD, in particular since next to leading order terms are included in the QCD predictions for these processes [3, 4].

Experimentally it is difficult to measure the production of direct photons in the presence of the much more copious π^0 and η production at large p_T , since unrecognized $\pi^0 \rightarrow \gamma\gamma$ and $\eta \rightarrow \gamma\gamma$ decays lead to a large background. In order to suppress this background it is necessary to identify and reconstruct for each event π^0 's and η 's with high efficiency. To satisfy this requirement a large acceptance photon detector with high spatial resolution for electromagnetic showers was built for this experiment. Because of the small cross sections expected, the detector was constructed to operate in an intense particle beam ($\sim 10^7$ particles/sec) of the SPS at CERN. Several trigger levels including a trigger processor allowed to select large p_T electromagnetic showers with a trigger reduction rate of 1 in 10^5 interactions.

A list of publications describing preliminary results of this experiment is given in ref. [5]. Recently other fixed target experiments have also published results on this subject [6].

The paper is organized in the following manner: Sect. 2 contains a description of the apparatus and the trigger, sect. 3 a discussion of the analysis procedure, sect. 4 presents the experimental results and sect. 5 gives the summary.

2. Apparatus and Trigger

The layout of the apparatus is shown in Fig. 1. A 300 GeV/c momentum beam of negative or positive charge with up to 10^7 particles/sec impinged on a 1 m liquid hydrogen target. Protons and pions in the beam were identified using two CEDAR Cerenkov counters. The negatively charged beam was a nearly pure π^- beam, whereas the content of π^+ in the positively charged beam was only 13 %. An iron wall and a veto counter array positioned upstream of the detector were used to reduce the trigger rate due to upstream interactions and muon background. Charged particles were detected by a proportional wire chamber telescope of 10 planes with $1 \times 1 \text{ m}^2$ and 12 planes with $2 \times 2 \text{ m}^2$ area [7]. A fine grained photon position detector (PPD) of 9.6 radiation lengths (X_0) measured the impact point and the lateral and longitudinal energy deposition of electromagnetic showers [8]. It was followed by a 240 cell ring calorimeter consisting of a 16 X_0 lead/scintillator sandwich photon section and a 6 absorption length (λ_a) iron/scintillator sandwich hadron section [9]. The acceptance of the calorimeters ranged between -0.8 and +0.8 in c.m.s. rapidity and covered 2π in azimuth. The energy flow through the 56 cm diameter central hole of the ring calorimeter was measured by a downstream calorimeter [9].

The front of the fine grained photon position detector (Fig. 2) was located 8.12 m downstream of the center of the H_2 target. Its four quadrants covered an area of $3 \times 3 \text{ m}^2$ excluding a central hole of $0.5 \times 0.5 \text{ m}^2$. The detector consisted of alternate layers of 1.1 X_0 lead sheets and proportional tubes of triangular cross-section with a wire spacing of 0.773 cm oriented vertically, horizontally and with an inclination of $\pm 45^\circ$. The signals from two successive layers of horizontal or respectively vertical tubes were summed and read out using ADC's. The 45°

wire planes were equipped with digital read out only. The PPD and the photon section of the ring calorimeter were also read out with Flash ADC's in a coarser granularity. Their data were used on line by the trigger processor and off line to eliminate background by the precise time information.

The proportional tubes and their electronic chains were individually calibrated with a ^{109}Cd source (22keV). The homogeneity was checked with horizontal beam scans across the PPD. The variations were found to be $\pm 2\%$. A gas pressure regulation system was employed to stabilize the density of the gas in the proportional tubes reducing the gain variation to less than $\pm 2\%$. The calorimeter system was calibrated with electrons from 5 to 170 GeV and hadrons from 10 to 60 GeV. The energy was determined as a weighted sum of the signals from the PPD and the ring calorimeter. The weights were chosen to give the best linearity over the full energy range. The obtained energy resolution for incident electrons was $\sigma/E = 0.28/\sqrt{E/\text{GeV}}$. A final calibration correction of at most 5% was obtained by normalising the reconstructed π^0 and η mass to the expected values. The normalisation to the π^0 or η mass differed by 1%. We therefore assigned an energy and p_T -scale uncertainty of $\pm 1\%$.

Various trigger levels were necessary to reduce the overall deadtime of the system. Events were on-line selected by the following sequence of triggers:

- a.) an interaction trigger (minimum bias) consisting of a small 3 cm diameter veto counter behind the proportional chambers.
- b.) a PPD pretrigger, with a low p_T threshold, using pulse height information from PPD strips. One strip contained the electronically added signals of a region which was 16 proportional wire tubes wide. Adjacent strips had an overlap region of 8 wires.
- c.) a PPD plus ring calorimeter trigger, with a medium p_T threshold. The threshold was applied to the electronically added sum of p_T -weighted signals from ring calorimeter cells within 30° azimuthal sectors and of the p_T -weighted signals from PPD strips which exceed a certain energy threshold (linear gates).
- d.) a trigger processor (for each quadrant) with a high p_T threshold, which used the Flash-ADC information of the PPD strips and of clusters of ring

calorimeter cells to compute the energy of electromagnetic clusters at the intersection of the PPD strips. If the energy exceeded the threshold value in a look up table, the event was accepted [10].

Data were taken at various p_T thresholds to cover the full p_T range accessible. At the highest trigger threshold of $p_T > 3.75$ GeV/c the system was taking data with an incident beam intensity of 10^7 particles per sec, a trigger reduction of 1 event in 10^5 interactions and a dead time of < 20 %.

Parallel to the single photon trigger an additional trigger at a lower p_T threshold in levels (c, d) was implemented in order to select two photon final states. This trigger required two electromagnetic clusters with a $p_T \geq 2$ GeV/c each to occur in neighbouring or opposite quadrants. The analysis of these events will be published elsewhere.

3. Analysis

The sensitivity of the experiment was 1330, 190 and 450 events per nanobarn for $\pi^- p$, $\pi^+ p$ and pp collisions respectively. The relatively low sensitivity obtained for $\pi^+ p$ collisions is explained by the low content of pions ($\sim 13\%$) in the positively charged beam at 300 GeV/c.

First we removed events which occurred outside the target, triggers from halo muons decaying between the upstream iron absorber wall and the calorimeters and pileup background. The events were passed through a program which reconstructed the tracks in the proportional chamber telescope and the vertex position. Only events with more than 3 tracks pointing to a vertex inside the 0.7 m fiducial length of the hydrogen target were retained. This multiplicity cut removed less than 1.5% of the genuine events. Next, the direction of the triggering electromagnetic shower was determined from the shower position in the front and the back parts of the PPD. Background trigger particles traveling parallel to the incident beam could thus be distinguished from genuine particles coming from the H_2 target. In a further cut the total energy sum of all calorimeters was required to be consistent with the beam energy. Finally the timing of the triggering shower obtained from the 30 MHz Flash-ADC information had to coincide with the beam interaction in the target. The histograms in Fig. 3 show for triggering electro-

magnetic showers with $p_T > 4$ GeV/c the distributions of the measured shower direction (a), total energy (b) and time center of gravity of the calorimeter signal (c). The shaded histograms show those events which satisfy the cuts indicated in the other two histograms. We conclude that the background is efficiently removed by the combined selections.

In the next analysis step, photon showers were reconstructed. The program searched for energy clusters in the horizontal and vertical projections of each quadrant and combined them to showers in space according to the correlation in energy and shower development. The parameters describing these correlations have been extracted from calibration data. Then the program distributed the energy found in the corresponding ring calorimeter cells to these showers. The two photon effective mass spectrum of those combinations containing the trigger shower are plotted in Fig. 4 and 5 showing the π^0 and η mass peaks with a mass resolution of $\sigma_{m_{\pi^0}} = 16$ MeV and $\sigma_{m_{\eta}} = 30$ MeV. If a pair of photons was found with an invariant mass between 55 and 210 MeV (470 and 620 MeV) it was assigned to originate from a π^0 (η) decay. An electromagnetic shower which could not be paired to form a π^0 or η and had a width consistent with a single shower was considered a direct photon candidate. In the following p_T refers to the transverse momentum of the photon, the π^0 and the η respectively.

A Monte Carlo event generator was used to estimate the detection efficiency of π^0 , η and direct photons, the background to the direct photon candidates and the effects of the finite energy resolution of the calorimeters on the cross sections. This Monte Carlo program generated π^0 , η and direct photon events with rapidity and p_T distributions as parameterized in reference [11]. It utilized showers obtained from tagged photon and electron beam calibration runs to simulate the detector response. The Monte Carlo events were then analysed with the same shower reconstruction program as the data.

The agreement between the Monte Carlo generated events (shown as curves) and the data (shown as histograms) is illustrated for the following quantities:

- i) the two photon invariant mass distributions in the π^0 and η mass region in Fig. 4 and 5 respectively,
- ii) the distribution of the separation of the two photon showers from π^0 decay

at the PPD for events with $p_T > 5$ GeV/c in Fig. 6.

- iii) the shower width distribution of direct photon candidates with $p_T > 4$ GeV/c in Fig. 7. For comparison also the Monte Carlo result for coalesced π^0 decay showers is shown by the dotted curves.
- iv) the asymmetry distribution of reconstructed π^0 decays in Fig. 8, where the asymmetry is defined by $A = \frac{|E_1 - E_2|}{E_1 + E_2}$ with E_1 and E_2 being the energies of the decay photons.

The background to the direct photon candidates, estimated with the Monte Carlo program, is shown in Fig. 9. It is mainly due to:

- a) photons from π^0 and η decays, for which one of the photons escapes detection in the PPD because of its limited geometrical acceptance. This background is decreasing with increasing p_T .
- b) photons from π^0 and η decays, for which one of the photons escapes detection in the photon detector because the reconstruction program is inefficient for photon energies below 2 GeV. This background is also decreasing with increasing p_T .
- c) coalesced showers from π^0 decays. For π^0 's with shower separation of less than 3 cm the reconstruction efficiency is decreasing due to coalescing showers. Therefore a shower width cut at 1.84 cm was applied for photon energies above 75 GeV. In this way 90% of all single photon showers with $p_T > 5.5$ GeV/c (70 % of showers with energy greater than 75 GeV) were retained and 70% of the coalesced showers rejected. The remaining background from coalescing showers starts to be significant at $p_T > 5$ GeV/c and increases with p_T . Decays of $\eta \rightarrow \gamma\gamma$ do not contribute to this background because of their large decay angles.

Possible other background sources like $\omega \rightarrow \pi^0\gamma$, $\eta' \rightarrow \rho^0\gamma$ etc. were neglected because of their small branching ratios and trigger acceptance.

The uncorrected ratio of direct photon candidates to π^0 's is shown in Fig. 10 for π^-p collisions. The hatched area indicates the Monte Carlo estimated background and its systematic uncertainty. This uncertainty of $\pm 2\%$ was estimated from a comparison of the asymmetry distributions for reconstructed π^0 's from the data and the Monte Carlo (Fig. 8).

In order to eliminate edge effects in the calorimeters the geometrical acceptance was restricted to a region from -0.65 to $+0.52$ in c.m.s. rapidity, i.e. π^0 's, η 's and the direct photon candidates were required to hit the calorimeter at a radius between 39 and 126 cm. Also strips of 16 cm width, centered on the connecting edges of the PPD quadrants, were excluded.

After background subtraction the direct photon yields were corrected for acceptance, detection efficiency and finite energy resolutions of the calorimeters.

4. Results

Here we present and discuss only the results on the direct photon cross sections. Results on π^0 production cross sections are given in a separate paper.

The direct photon production cross sections measured in π^-p , π^+p and pp collisions at 300 GeV are listed in table I and plotted in Fig. 11 as a function of p_T . The cross sections are fully inclusive since no isolation criteria on the single photon candidates were applied. The statistical errors are shown as bars and the linear sum of the statistical and the systematic errors resulting from the uncertainties in the background subtraction as brackets. In addition to these errors there is a p_T scale uncertainty of $\pm 1\%$ and a normalisation uncertainty of $\pm 7\%$ in the cross section determination which is mainly due to the applied total energy cut.

The curves in Fig. 11 show the results of higher order QCD calculations [3, 12].* The agreement with our experimental results is rather good considering the remaining systematic uncertainties in the experiment and the uncertainties in the theoretical predictions.

*The proton and pion structure functions were taken in the two parametrisations of reference [13]. The solid curves represent the results of the QCD calculation using the structure functions of set 1 with $\Lambda = 0.2$ GeV of reference [13] and the dashed curves of set 2 assuming harder gluon distributions with $\Lambda = 0.4$ GeV. In these calculations the dependence of the cross sections on the factorisation and renormalisation scale variables were minimized according to "the principle of minimal sensitivity" [14]. The resulting scale variables come out to be approximately $0.35 p_T^2$. To illustrate the dependence of the predicted cross sections on the choice of scale variables we also did a calculation with structure function set 1 and fixed scale variables of $4 p_T^2$ (dashed dotted curves).

The γ/π^0 cross section ratios in π^-p , π^+p and pp collisions are plotted in Fig. 12. As expected all reactions show a rising ratio with increasing p_T . This suggests that direct photons at large p_T are radiated from interacting quarks and are not products of quark or gluon fragmentations as for example π^0 's are.

The ratio of the direct photon cross sections in π^-p and π^+p collisions together with the QCD predictions of ref. [3] (shown as line) and ref. [4] (shown as the hatched region) are plotted in Fig. 13. In this case the systematic errors due to the background subtraction are evaluated assuming correlated systematic errors in the π^-p and π^+p cross sections. Not included are the p_T scale uncertainty and the normalisation uncertainty quoted above. Their effect however is expected to be small since the cross section ratio $\sigma(\pi^-p \rightarrow \pi^0 X)/\sigma(\pi^+p \rightarrow \pi^0 X)$ is close to unity. The rise of this ratio with increasing p_T signals the occurrence of valence quark antiquark annihilations.

Finally the cross section for direct photons produced in π^-p collisions at $p_T = 5$ GeV/c is shown in Fig. 14 as a function of the c.m.s. rapidity together with the QCD prediction of reference [3]. The distribution is peaked towards positive rapidities reflecting the harder momentum spectrum of the quarks and gluons in the pion compared to those in the proton.

5. Summary

Direct photon production cross sections were measured in π^-p , π^+p and pp collisions at 300 GeV/c. The increase of the cross section ratio $\sigma(\pi^-p \rightarrow \gamma X)/\sigma(\pi^+p \rightarrow \gamma X)$ with p_T indicates the occurrence of valence quark-antiquark annihilations. The results are well described by QCD calculations.

6. Acknowledgements

We are grateful for the excellent technical help provided by R. Ferorelli, H. Fessler, W. Fröchtenicht, B. Gordeev, M. Kellner, M. Mongelli, H.J. Osthoff, M. Perchiuzzi, H. Röser, A. Sacchetti, J. Seyboth and V. Vinogradov. We wish to thank the staff at CERN for the operation of the SPS accelerator and the H2 beam line and the supporting help of the SPS coordinators.

REFERENCES

- [1] H. Fritzsch, P. Minkowski, Phys. Lett. **69B** (1977) 316
- [2] M. Diakonou et al., Phys. Lett. **87B** (1979) 292;
R. Baltrusaitis et al., Phys. Lett. **88B** (1979) 372;
A.L.S. Angelis et al., Phys. Lett. **94B** (1980) 106;
T. Akesson et al., Phys. Lett. **123B** (1983) 367;
M. McLaughlin et al., Phys. Rev. Lett. **51** (1983) 971.
- [3] P. Aurenche et al., Phys. Lett. **140B** (1984) 87; Z. Phys. **C29** (1985),
459 and private communication;
R. Baier, private communication
- [4] A.P. Contogouris et al., preprint 1985 and private communication
- [5] K. Pretzl, Proc. of the XII International Conference on High Energy
Physics, Leipzig, Vol. 1 (1984) 283;
P. Seyboth, XV International Symposium on Multiparticle Dynamics,
Lund (1984) page 596;
A. Bamberger, Proc. of the XX Rencontre de Moriond (1985) 201;
K. Pretzl, XVI International Symposium on Multiparticle Dynamics,
Kiryat- Anavim (1985) page 149.
- [6] J. Badier et al., Z. Phys. **C31** (1986) 341;
E. Lancon, Proc. of the XXI Rencontre de Moriond, Vol.2 (1986) 101.
- [7] M. De Palma et al., NIM **217** (1983) 135,
A. Weltin, Diplomarbeit (1982) Freiburg University, unpublished
- [8] V. Artemiev et al., NIM **224** (1984) 408.
- [9] C. De Marzo et al., NIM **217** (1983) 405.
- [10] to be published later.
- [11] G. Donaldson et al., Phys. Lett. **73B** (1978) 375.

- [12] For the numerical calculations we used a program which the authors of ref. [3] kindly provided.
- [13] D.W.Duke and J.F. Owens, Phys. Rev. **D30** (1984) 49;
and J.F. Owens, Phys. Rev. **D30** (1984) 943.
- [14] P. Aurenche et al., Invited talk given at the VII International Workshop on Photon-Photon Collisions (College de France, Paris, 1.-5. April 1986) LAPP-TH-159 and LPTHE Orsay 86/14.

Table 1

Invariant cross sections for direct photon production averaged over the c.m.s. rapidity region from -0.65 to 0.52. The first errors are statistical, the second errors are systematic due to the uncertainties in the background subtraction procedure. In addition there is a $\pm 1\%$ uncertainty in the p_T scale and a $\pm 7\%$ uncertainty in the normalisation.

p_T (GeV/c)	$E \cdot \frac{d^3\sigma}{dp^3} (\text{cm}^2 \cdot \text{GeV}^{-2} \cdot \text{c}^3)$		
	$pp \rightarrow \gamma + X$	$\pi^+ p \rightarrow \gamma + X$	$\pi^- p \rightarrow \gamma + X$
2.75			$(3.03 \pm 0.49 \pm 0.70) \cdot 10^{-33}$
3.25	$(3.75 \pm 0.93 \pm 1.70) \cdot 10^{-34}$	$(7.72 \pm 1.50 \pm 1.60) \cdot 10^{-34}$	$(7.78 \pm 0.69 \pm 1.70) \cdot 10^{-34}$
3.75	$(1.21 \pm 0.39 \pm 0.29) \cdot 10^{-34}$	$(3.10 \pm 0.76 \pm 0.39) \cdot 10^{-34}$	$(2.94 \pm 0.34 \pm 0.36) \cdot 10^{-34}$
4.25	$(2.50 \pm 0.40 \pm 0.75) \cdot 10^{-35}$	$(5.42 \pm 0.87 \pm 0.79) \cdot 10^{-35}$	$(8.93 \pm 0.34 \pm 0.88) \cdot 10^{-35}$
5.00	$(5.48 \pm 1.20 \pm 1.10) \cdot 10^{-36}$	$(1.00 \pm 0.25 \pm 0.25) \cdot 10^{-35}$	$(2.10 \pm 0.11 \pm 0.22) \cdot 10^{-35}$
6.00	$(9.50 \pm 3.90 \pm 0.60) \cdot 10^{-37}$	$(8.31 \pm 5.70 \pm 1.20) \cdot 10^{-37}$	$(2.55 \pm 0.34 \pm 0.13) \cdot 10^{-36}$
7.00			$(3.69 \pm 1.40 \pm 0.12) \cdot 10^{-37}$

FIGURE CAPTIONS

1. Layout of the NA24 experiment.
2. Overview of the calorimeter system with a blown up section of the photon position detector (PPD).
3. Distributions for (a) the shower direction of the highest p_T cluster (R is the distance of the impact point from the beam, ΔR the radial displacement between the position in the front and the back of the PPD) (b) the total energy sum and (c) the timing of the high p_T cluster. These distributions are from a sample of triggering electromagnetic showers with $p_T > 4$ GeV/c in π^-p collisions. The shaded histograms show those events which satisfy the cuts indicated in the other two histograms.
4. Two photon invariant mass spectrum in the π^0 mass region with $4 < p_T < 5$ GeV/c. The distribution has a σ of 16 MeV. The solid curve gives the result of the Monte Carlo simulation (due to the cuts in the reconstruction procedure the mass values come out somewhat lower than the true values).
5. Two photon invariant mass spectrum in the η mass region with $3 < p_T < 4$ GeV/c. The η mass peak has a σ of 30 MeV. The solid curve gives the result of the Monte Carlo calculation, the dashed line is an estimate of the combinatorial background (due to the cuts in the reconstruction procedure the mass values come out somewhat lower than the true values).
6. Distribution of the separation of the two photons from reconstructed π^0 decays with $p_T > 5$ GeV/c at the PPD. The solid line is the result of the Monte Carlo calculation.
7. Distribution of the r.m.s. shower width of photon candidate showers with $p_T > 4$ GeV/c. The full curve is the result of the Monte Carlo calculation for direct photon showers, the dashed curve for coalesced π^0 's.
8. Asymmetry distribution of reconstructed π^0 decays with $4 < p_T < 5$

GeV/c. The curve represents the result of the Monte Carlo simulation.

9. The ratio direct photon background from π^0 and η decays to the reconstructed π^0 yield as calculated by the Monte Carlo simulation. The solid curve represents the total background. It consists of contributions from η decays (dashed curve), π^0 decays where one photon is lost outside the detector (dashed dotted curve), π^0 decays where one photon is not reconstructed (dotted curve) and π^0 decays where the two photons coalesce into a single shower (dashed double dotted curve).
10. Ratio of yields of direct photon candidates to reconstructed π^0 's with asymmetry $A < 0.8$ in π^-p collisions versus p_T . The hatched region shows the Monte Carlo estimated background and its systematic uncertainty.
11. Invariant cross sections for inclusive direct photon production in π^-p , π^+p and pp collisions at 300 GeV/c versus p_T . See text for the explanation of the errors. The curves give the predictions from higher order QCD calculations [3]. The solid curves represent the results of the QCD calculation using the structure functions of set 1 with $\Lambda = 0.2$ GeV of ref. [13] and the dashed curves of set 2 assuming harder gluon distributions with $\Lambda = 0.4$ GeV. The dashed dotted curves are the result of a calculation with structure function set 1 and fixed scale variables $4p_T^2$.
12. Ratio of the inclusive direct photon cross section to the inclusive π^0 cross section for π^-p , π^+p and pp collisions versus p_T .
13. Ratio of the direct photon cross sections in π^-p and π^+p collisions versus p_T and x_T , with $x_T = \frac{2p_T}{\sqrt{s}}$. For the explanation of the errors see text. The solid curve ref. [3] and the hatched region ref. [4] give the results of two QCD predictions.
14. Invariant direct photon cross section for π^-p interactions as a function of the photon c.m.s. rapidity at $p_T = 5$ GeV/c. The curve shows the result of the higher order QCD calculation of ref. [3]. See text for the explanation of the errors.

LAYOUT NA-24

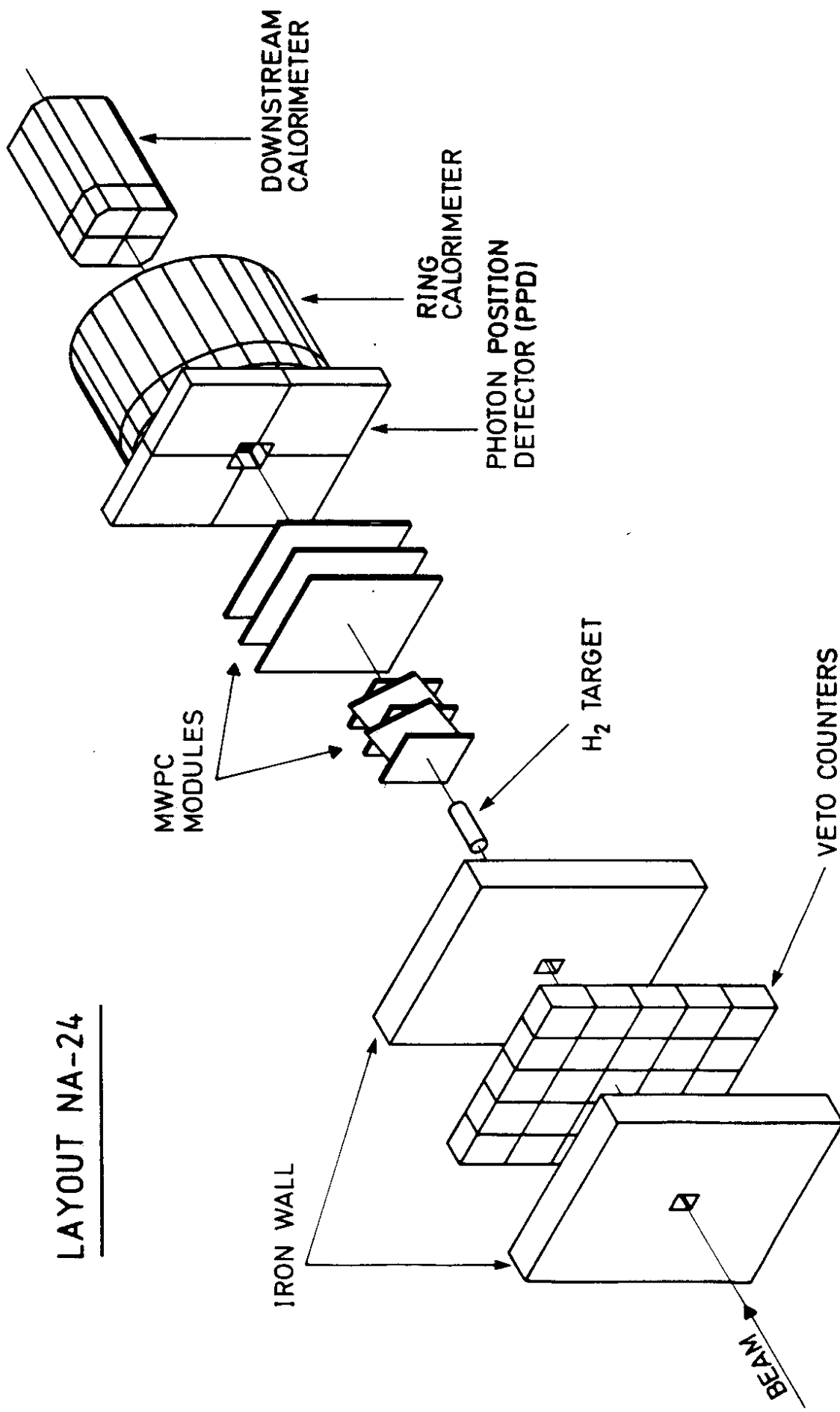


Fig. 1

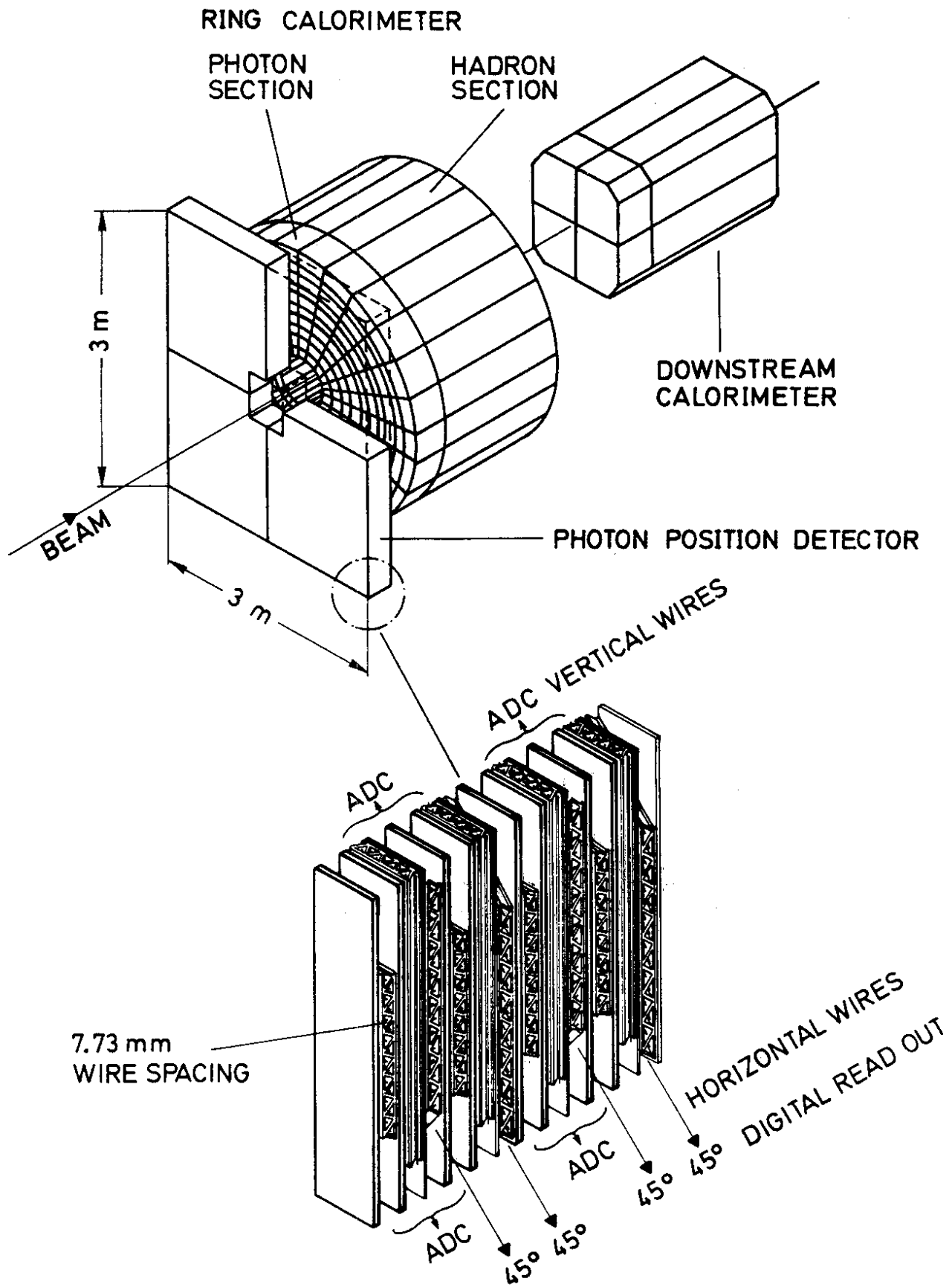


Fig. 2

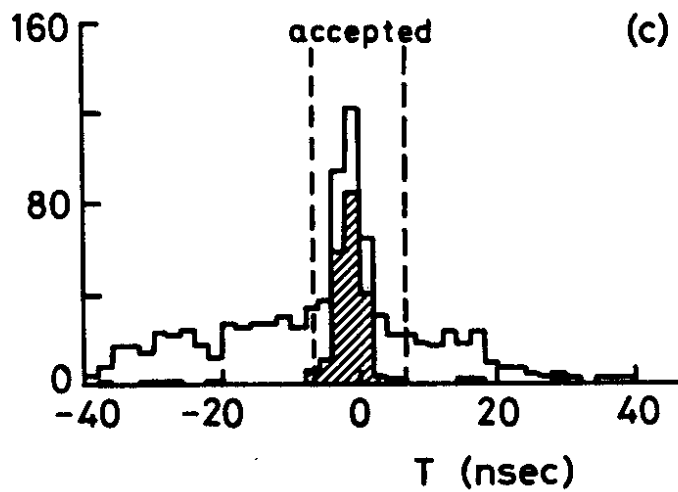
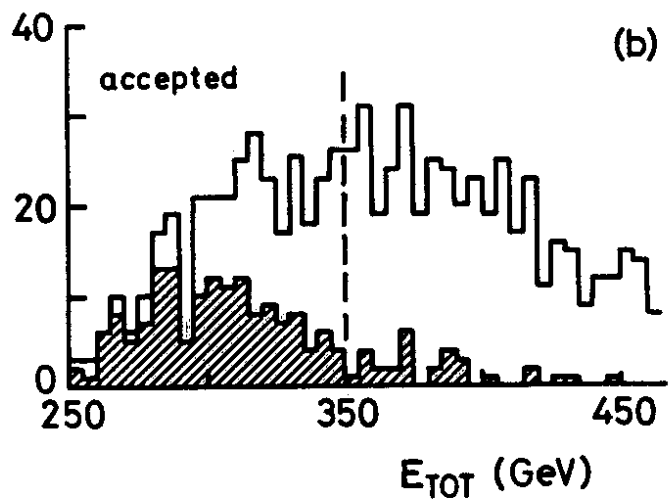
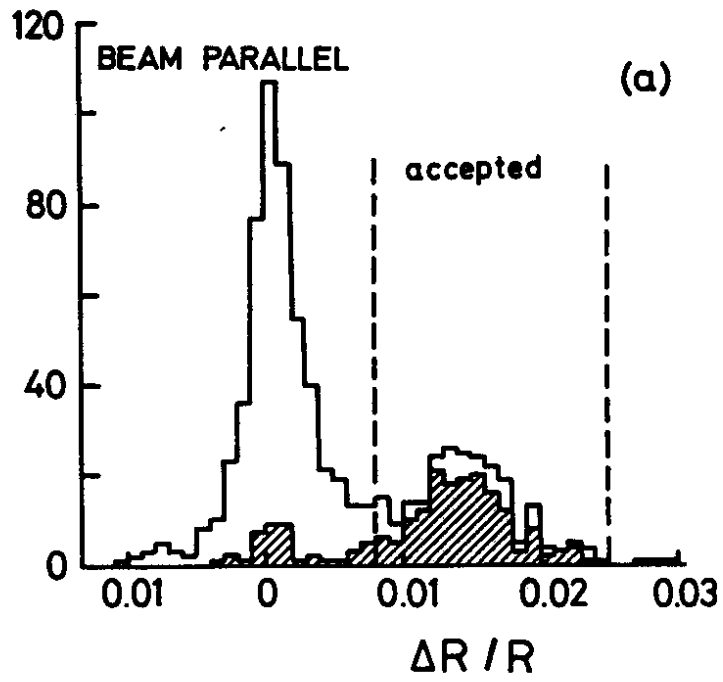


Fig. 3

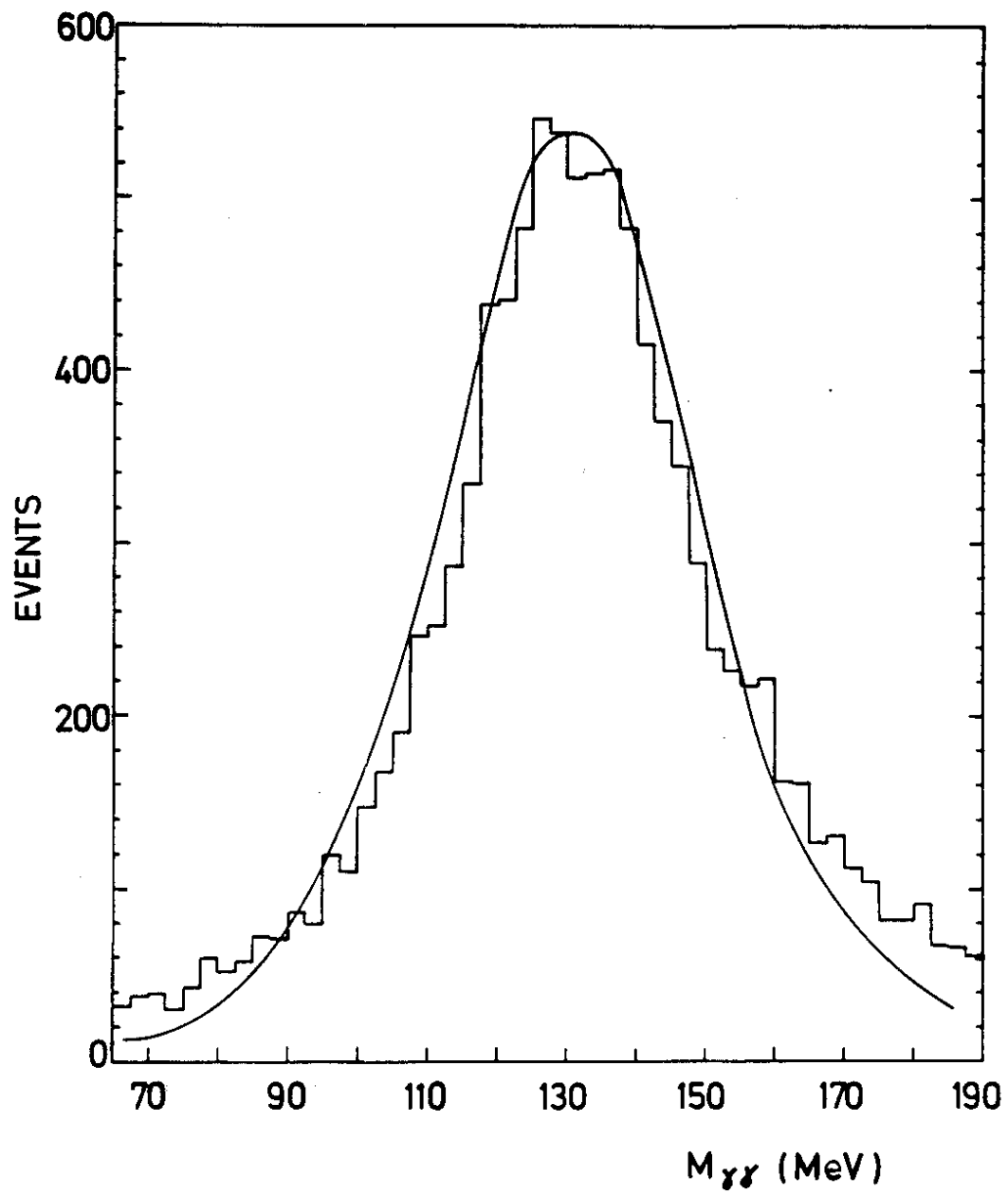


Fig. 4

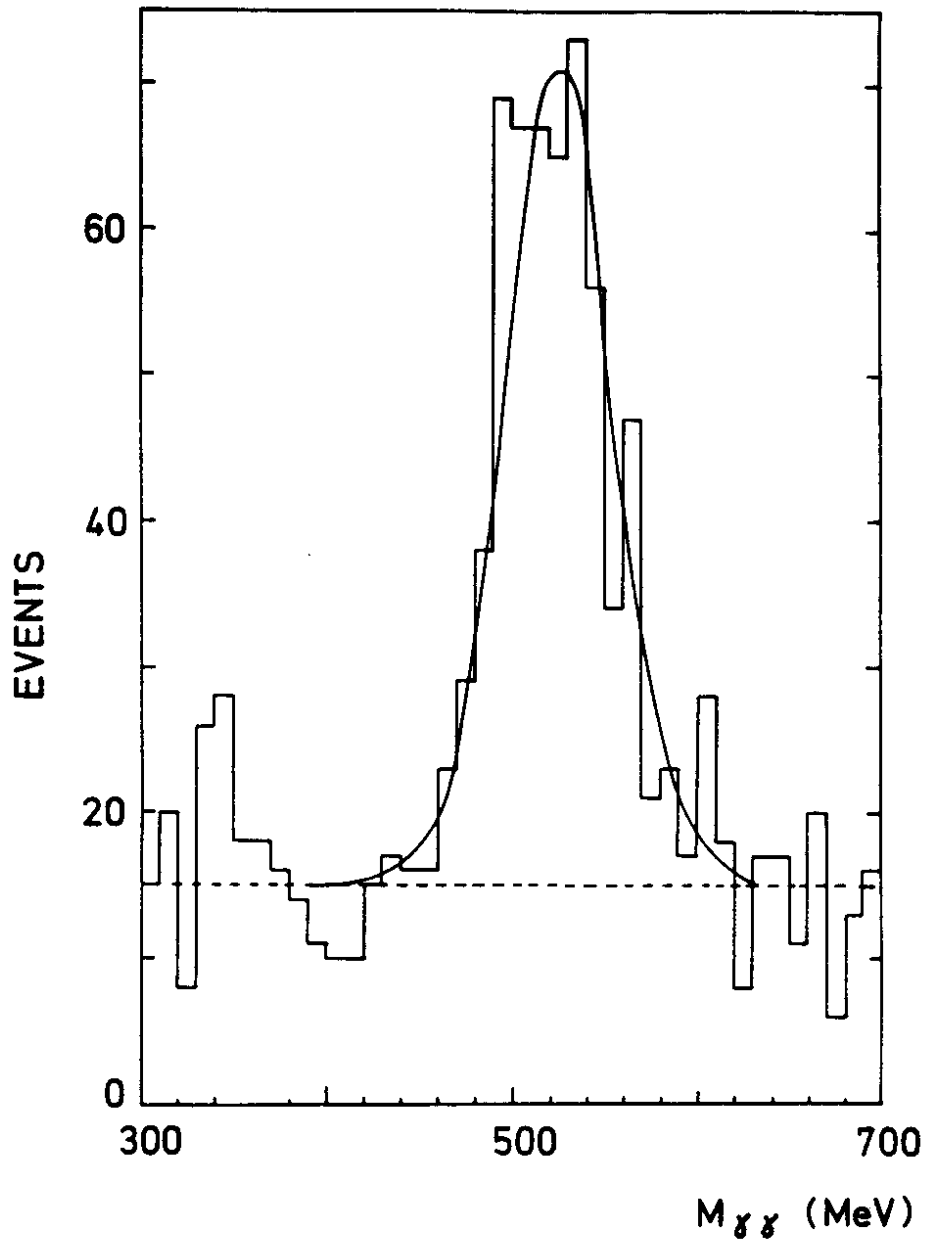


Fig. 5

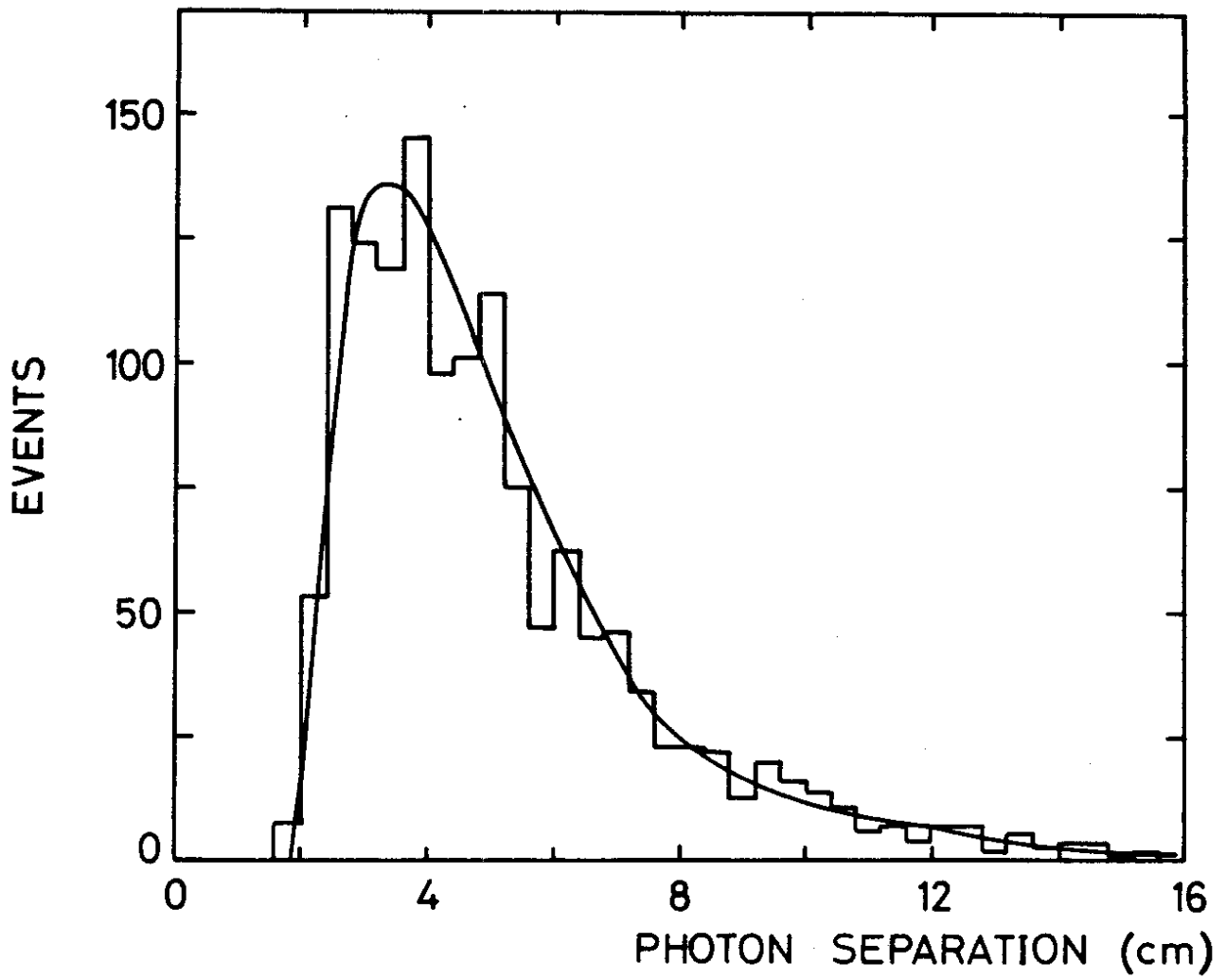


Fig. 6

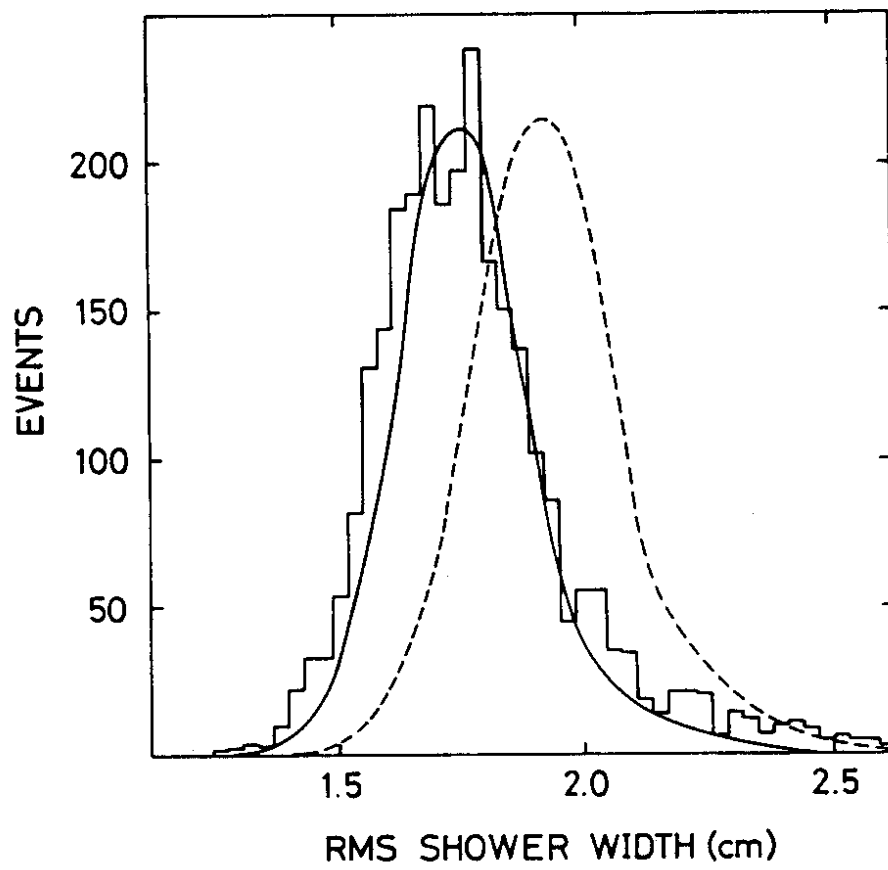


Fig. 7

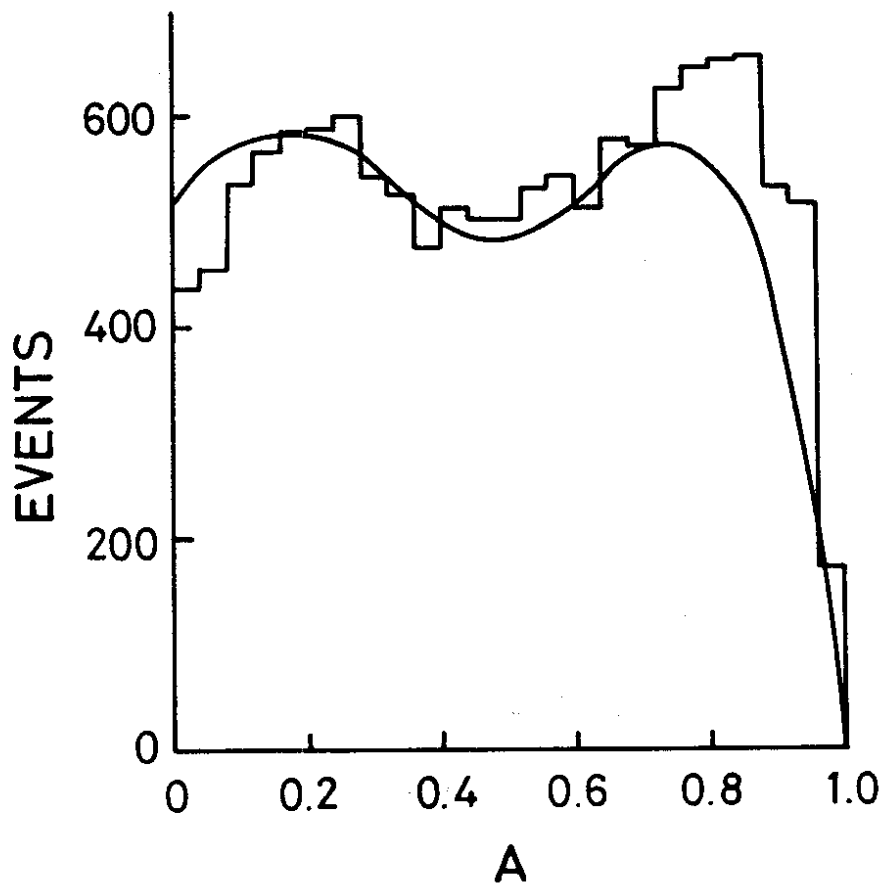


Fig. 8

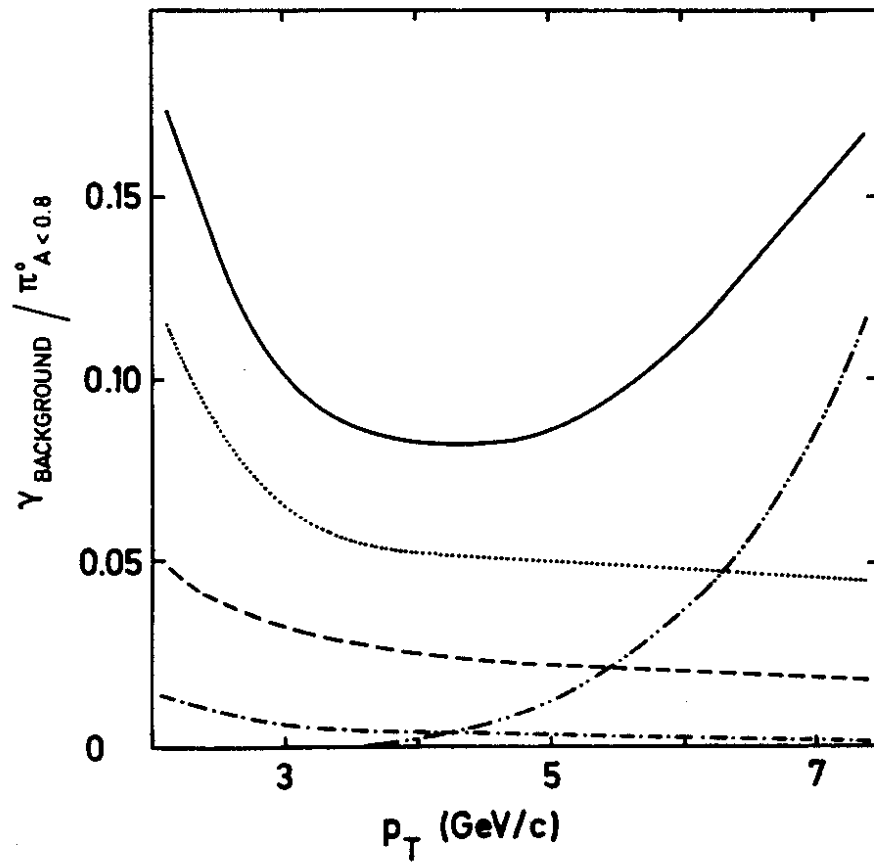


Fig. 9

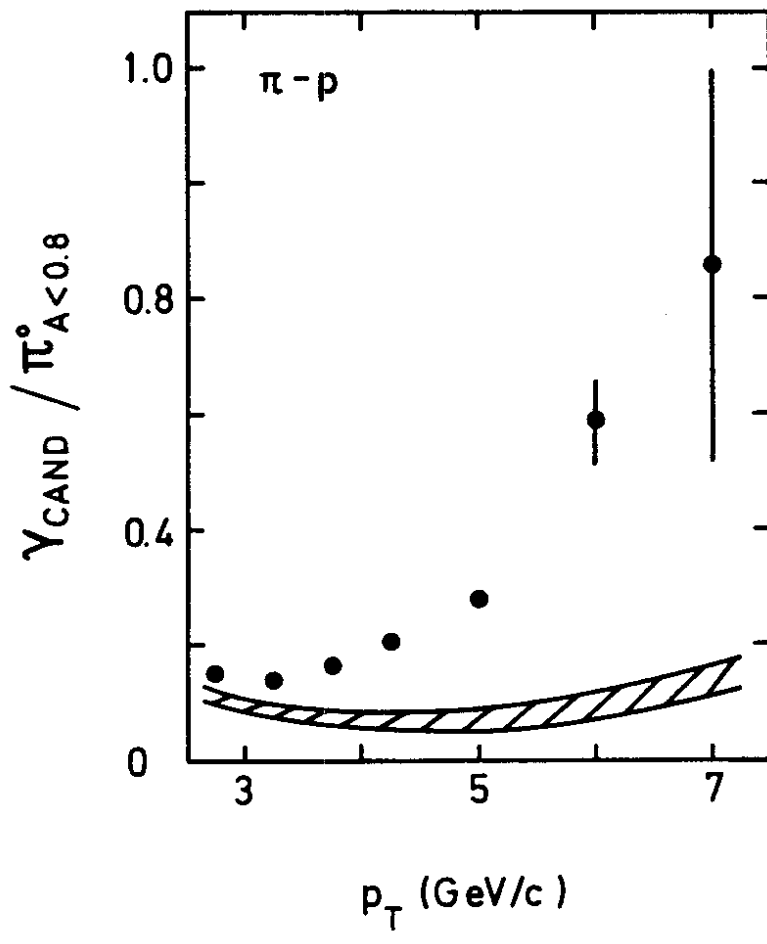


Fig. 10

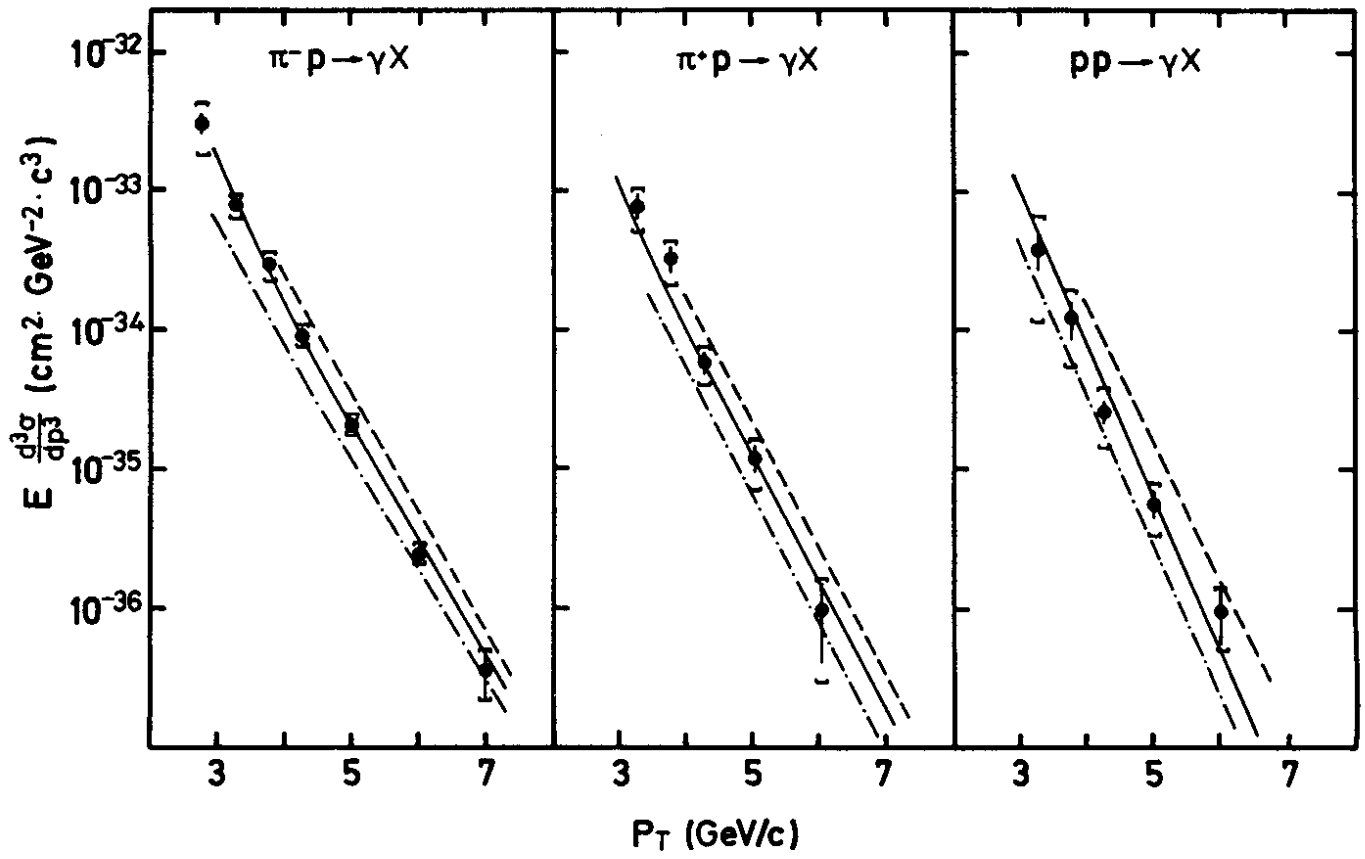


Fig. 11

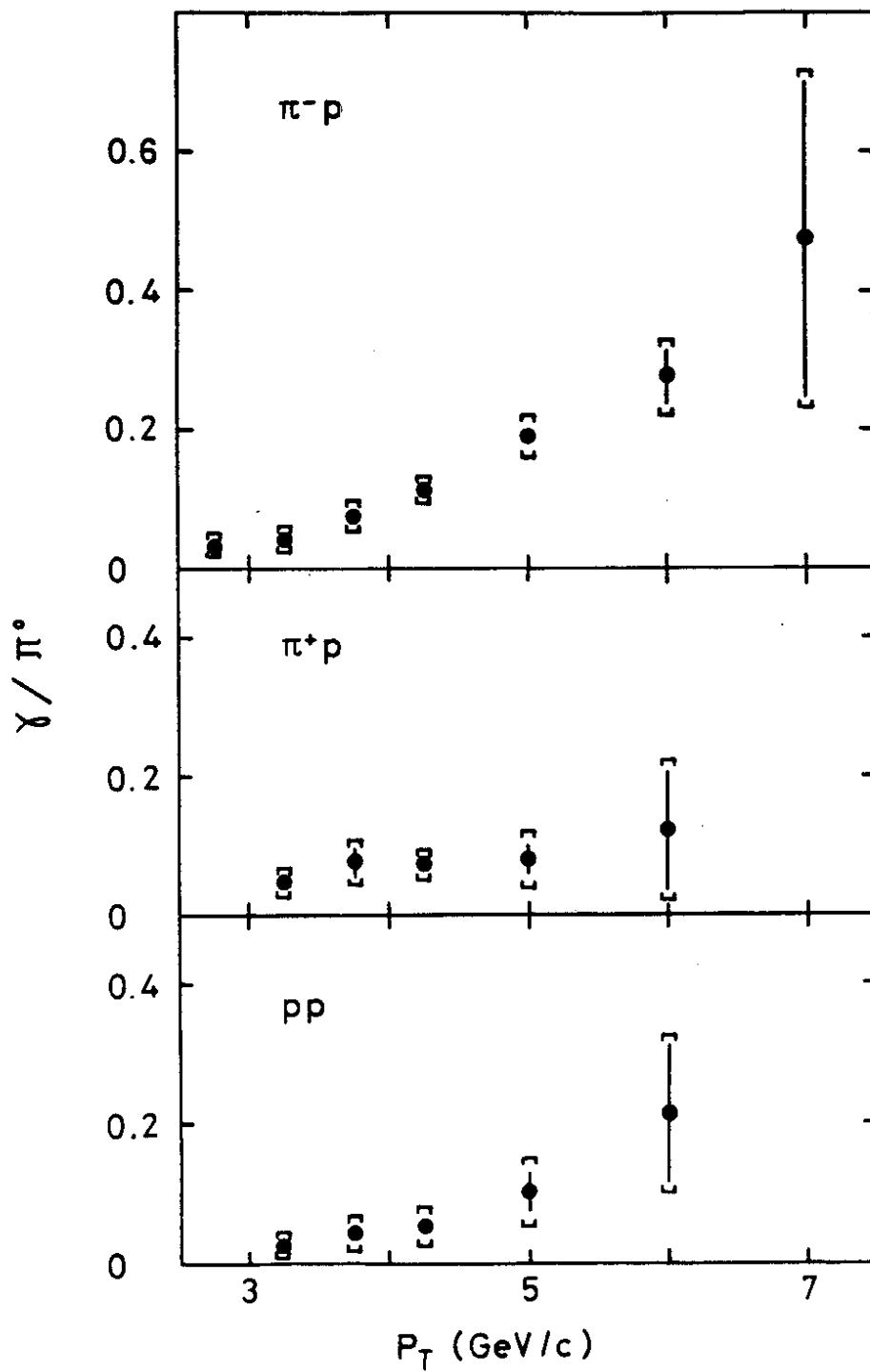


Fig. 12

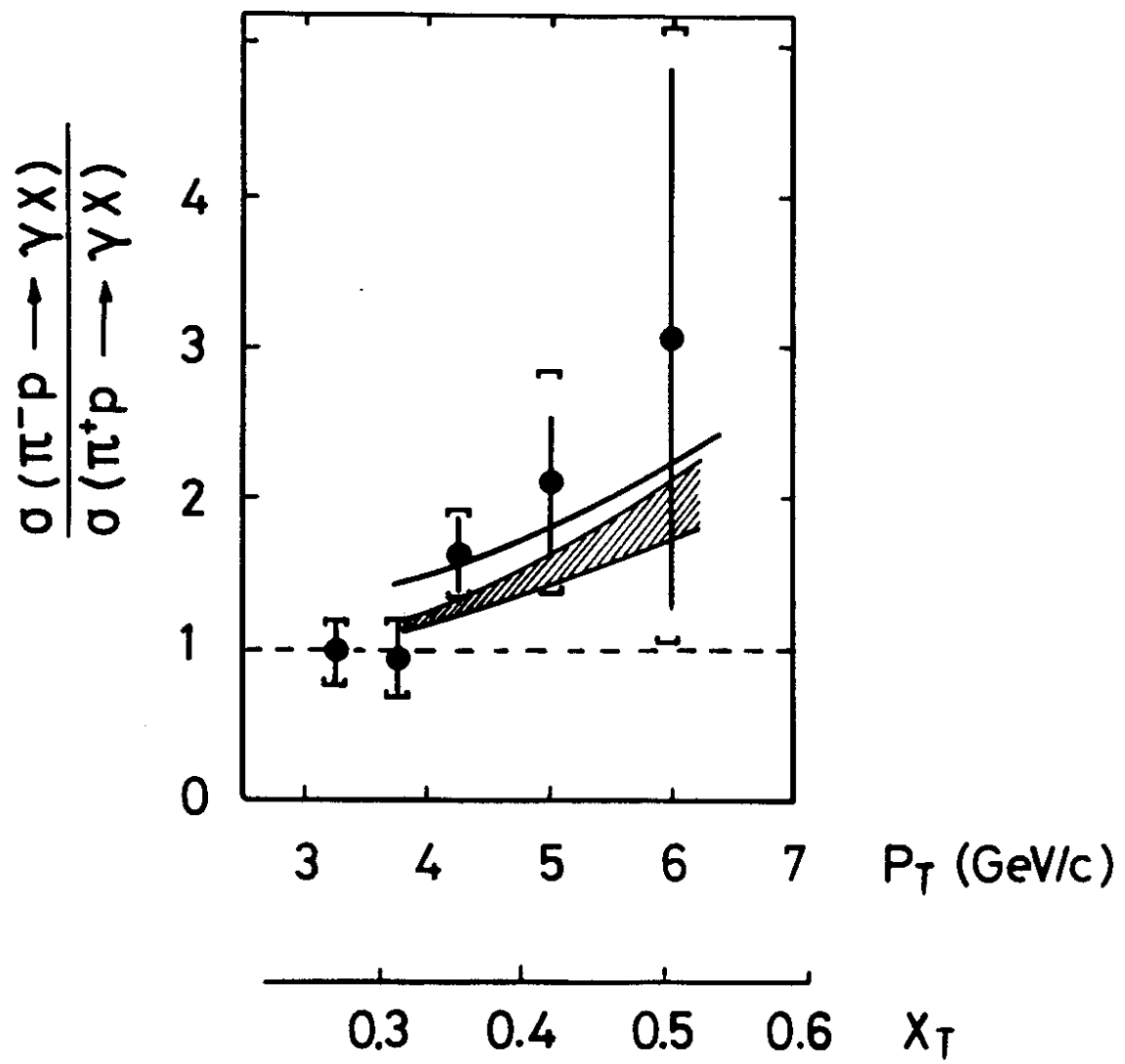


Fig. 13

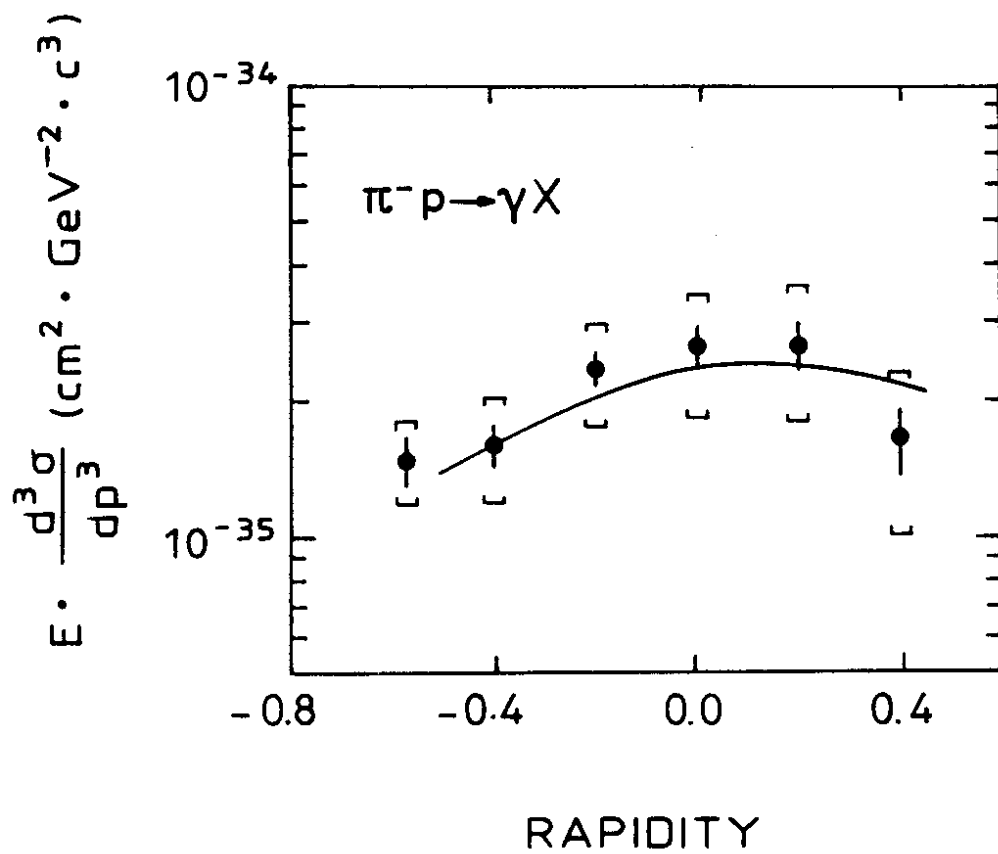


Fig. 14

